

## A NEW MECHANICAL FRAMEWORK TO INTERPRET WEAK LAYER AND SLAB FRACTURE IN THE PROPAGATION SAW TEST

Lorenzo Benedetti<sup>1,2\*</sup>, Jan-Thomas Fischer<sup>1</sup> and Johan Gaume<sup>3,4</sup>

<sup>1</sup>BFW – Austrian Research Centre for Forests, Department of Natural Hazards, Innsbruck, Austria

<sup>2</sup>CIMNE – International Center for Numerical Methods in Engineering, Barcelona, Spain

<sup>3</sup>WSL Institute for Snow and Avalanche Research SLF, Davos, Switzerland

<sup>4</sup>EPFL – École Polytechnique Fédérale de Lausanne, Lausanne, Switzerland

**ABSTRACT:** This work aims to provide a mechanical model for the Propagation Saw Test (PST) based on the Euler-Bernoulli beam, allowing a description of the slab and weak layer stress states in the quasi-static regime. We assume an elastic-perfectly brittle model as constitutive law for both the snow slab, which can fracture for high tensile stresses, and the weak layer, which can fail under compressive or shear stress. The stress evolution is mainly determined by the crack length, which is initially created by the saw and, subsequently, increases due to weak layer failure in case of self-propagation. Thanks to the proposed method, the two main test outcomes -full propagation (END) and slab fracture (SF)- can be found as observed in field experiments. Moreover, the PST parameters can be studied separately, providing a powerful tool to understand the dependence of the outcome from numerous quantities in the test, both geometrical and mechanical.

**KEYWORDS:** fracture, critical length, propagation length, mechanical model

### 1. INTRODUCTION

In recent years, the Propagation Saw Test has drawn attentions being relatively easy to perform and providing useful insights for the evaluation of snow instability. Initially, this in-situ technique has been developed by Sigrist and Schweizer (2007) and Gauthier and Jamieson (2008) and, in the following years, numerous measurement were performed by van Herwijnen and Jamieson (2005) utilizing high speed PTV (particle tracking velocimetry). The results showed useful insights into the intricate relationships between the propagation of weak layer collapse and the upper slab deformation as well. The phenomenon has also been studied using Linear Elastic Fracture Mechanics theories by Heierli et al. (2008) while Schweizer et al. (2014) introduced an ad-hoc mechanical model. More recently, Gaume et al. (2015) employed the Discrete Element Method as a numerical tool to simulate the evolution of the PST and its outcome.

This work aims to provide a simple quantitative

tool for an exhaustive mechanical interpretation of the PST by means of well-known mathematical models in the field of continuum mechanics.

To begin with, we analyze the different force schemes in the PST in order to construct a mechanical model based on the Euler-Bernoulli beam in the quasi-static regime. With the assumption of elastic-perfectly brittle material we provide the failure conditions for the snow slab, subjected to tensile stresses, and for the weak layer, which considers the effect of compressive and shear loading. We derived the functions representing the stress evolution with respect to the crack length, which is artificially created by the saw and, in case of self-propagation, lengthened due to weak layer failure. The results for a realistic snowpack highlight the capability of the model to detect full propagation (END) and slab fracture (SF) outcomes as observed in field experiments.

### 2. PST BEAM MODEL

The PST is conducted with an isolated volume of snow of 30 centimeters of width and about 1-2 meters in length (Figure 1). We investigate the case of a snow slab (of total length  $l_{tot}$ ) on top of a rigid bed, with a weak layer in between, on a slope of angle  $\psi$ .

---

\* *Corresponding author address:*

Lorenzo Benedetti,  
BFW - Austrian Research Centre for Forests,  
Department of Natural Hazards,  
Rennweg, 1, 6020 Innsbruck, Austria  
email: lore.benedetti@gmail.com

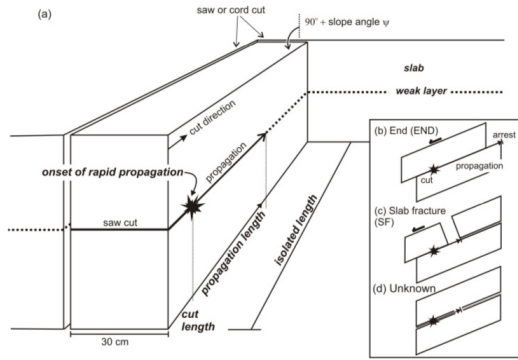


Fig. 1 : Propagation Saw Test setup and possible outcomes (from Gauthier and Jamieson, 2008)

First of all, we describe the sequence of events that takes place in the PST (Figure 2). At the beginning of the test, increasing the cut length  $l$  increases the load on the newly formed cantilever beam and on the reduced area of the weak layer, being both naturally subjected to the weight of the snow. The tip of the upper slab displaces -likewise vertically and horizontally- since the gravitational force is applied in a slanted direction with respect to the axis of the volume of snow (Scheme I).

The length  $L_{IC}$  is the value of  $l$  at which point we observe the first contact between the tip and the rigid bed and it is computed as:

$$L_{IC} = \sqrt[4]{\frac{8 E I h_w}{q_v}} \quad (1)$$

where  $E$  is the elastic modulus of the snow,  $I$  is the second moment of inertia of the upper slab cross section,  $h_w$  is the thickness of the weak layer and  $q_v$  is the vertical distributed load on the structure (measured in N/m). In this case, only the tip of the cantilever rests on the rigid bed, resulting in a hinged constrain, where the beam cross section can only rotate (Scheme II).

Then, following the increase of  $l$ , the slab bends back due to its own weight and rests having vertical cross section to the slope direction. At this point, not only any vertical movement is restrained, but also the rotation is forbidden. The cut length  $l$ , at which this condition is recognized, is called length of full contact and it is denoted by  $L_{FC}$  as:

$$L_{FC} = \sqrt[4]{\frac{72 E I h_w}{q_v}} = \sqrt{3} L_{IC} \quad (2)$$

When sawing is continued, the contact zone between the two slabs increases and the length be-

tween the saw and the first touching point remains constant, being equal to the full contact length  $L_{FC}$ , for equilibrium requirements. Finally, the beam is now behaving as a double clamped structure, with fixed length and, consequently, bending moment on the cross sections. In addition, the weight of the snow volume applied to the rigid bed causes friction effects which are exerted through the surfaces, modifying, hence, the horizontal equilibrium of forces (Scheme III).

In order to evaluate the stresses in the snowpack, it is required to solve the following differential equation for the Euler-Bernoulli beam:

$$\frac{d^2}{dx^2} \left[ E I \frac{d^2 v(x)}{dx^2} \right] + q(x) = 0 \quad (3)$$

in the function of vertical displacement  $v(x)$ . Similarly, the horizontal displacement  $u(x)$  is the solution of the second order differential equation:

$$\frac{d}{dx} \left[ E A \frac{du(x)}{dx} \right] + p(x) = 0 \quad (4)$$

Each force scheme provides the necessary boundary conditions required for the solution of the differential equations. Once the vertical and horizontal displacement functions are known, it is possible to calculate the stresses in the various layers of the snowpack. Concerning the upper slab, we assume an *elastic-brittle fracture* constitutive law, which means that the maximum tensile stress in the vertical cross section will provoke failure and detachment of the snow volume as soon as it reaches its threshold value. The bending moment  $M$  and the horizontal force  $N$  are combined in the Navier's formula to compute the maximum tensile stress in the upper slab:

$$\sigma_t^s = \frac{N}{bh} + \frac{6M}{bh^2} \quad (5)$$

where  $b$  is the width and  $h$  is the height of the upper slab. Likewise, assuming a rigid interface between the layers, the gravitational forces are transmitted to the weak layer and, with equilibrium arguments, we are able to compute the bending moment  $M_w$ , the normal force  $N_w$  and the shear force  $T_w$ . We assume an elastic-brittle behavior for the weak layer as well, which can reach failure for both compressive or shear stress. These values are calculated as:

$$\sigma_c^w = \frac{N_w}{b(l_{tot}-l)} + \frac{6M_w}{b(l_{tot}-l)^2} \quad (6)$$

$$\tau_s^w = \frac{T_w}{b(l_{tot}-l)} \quad (7)$$

In Figure 2, the resulting stress functions with respect to the saw cut length  $l$  are presented aside the corresponding force schemes.

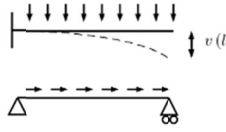
Knowing the evolution of stresses in the upper slab and the weak layer, it is possible to compare such values with their threshold stress and to compute the respective critical lengths  $l_c^s$  and  $l_c^w$ . Then, the (signed) propagation length, limited by the maximum specimen length  $l_{tot}$ , is found subtracting the latter two values as

$$l_p = \min(l_c^s - l_c^w, l_{tot}) \quad (8)$$

### 3. RESULTS

For the purpose of connecting the quantitative results to the outcome of the test, a PST example is now presented. In particular, varying the upper slab density  $\rho$ , the cases of full propagation (END) and slab fracture (SF) are recovered. In this test setup, the upper slab has an equal width and height of 30 centimeters. The total length of the specimen is 2 meters and the slope angle is  $35^\circ$ . Finally, the thickness of the weak layer is 1 millimeter and the static friction coefficient between the upper slab and the rigid bed is 0.5, equivalent to a friction angle of  $30^\circ$ .

Scheme I:  $l \leq L_{IC}$

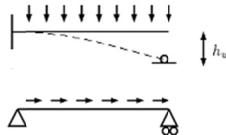


$$\sigma_t = \rho g h \left[ \frac{l}{h} \sin(\psi) + 3 \frac{l^2}{h^2} \cos(\psi) \right]$$

$$\sigma_c = \rho g h \cos(\psi) \frac{l_{tot}}{(l_{tot}-l)} \left[ 1 + \frac{3(l+h \tan(\psi))}{(l_{tot}-l)} \right]$$

$$\tau_s = \rho g h \sin(\psi) \frac{l_{tot}}{(l_{tot}-l)}$$

Scheme II:  $L_{IC} < l \leq L_{FC}$

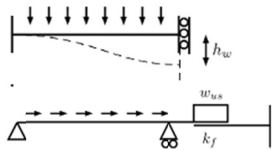


$$\sigma_t = \rho g h \left[ \frac{l}{h} \sin(\psi) + \frac{3}{4} \frac{l^2}{h^2} \cos(\psi) \left( 1 + 3 \frac{L_{IC}^4}{l^4} \right) \right]$$

$$\sigma_c = \rho g h \cos(\psi) \frac{l_{tot}}{(l_{tot}-l)} \left[ 1 - \frac{3l}{8l_{tot}} \left( 1 - \frac{L_{IC}^4}{l^4} \right) \left( \frac{2l_{tot}+l}{l_{tot}-l} \right) + 3 \frac{(l+h \tan(\psi))}{(l_{tot}-l)} \right]$$

$$\tau_s = \rho g h \sin(\psi) \frac{l_{tot}}{(l_{tot}-l)}$$

Scheme III:  $l > L_{FC}$



$$\sigma_t = \rho g h \left[ \frac{l}{h} \sin(\psi) - k_f \frac{l - L_{FC}}{h} \cos(\psi) + \frac{L_{FC}^2}{h^2} \cos(\psi) \right]$$

$$\sigma_c = \frac{3}{4} \rho g h \cos(\psi) \frac{L_{FC}}{(l_{tot}-l)} \left( 1 + \frac{1}{l_{tot}-l} \left[ 4h \frac{l_{tot}}{L_{FC}} \tan(\psi) - (l_{tot} - l - 2L_{FC}) \right] \right)$$

$$\tau_s = \rho g h \sin(\psi) \frac{l_{tot}}{(l_{tot}-l)} \left( 1 - k_f \frac{l - L_{FC}}{l_{tot} \tan(\psi)} \right)$$

Fig. 2 : Force schemes for the vertical and horizontal forces with the corresponding solution for the tensile stress  $\sigma_t$  in the upper slab, the compressive stress  $\sigma_c$  and the shear stress  $\tau_s$  in the weak layer. In the horizontal force schemes, the symbol  $k_f$  represents the static friction coefficient whereas  $w_{us}$  is the weight of the upper slab in contact with the rigid bed.

Regarding the maximum allowed stress values, the compressive strength of the weak layer is set to 2.5 kPa and the shear strength to 0.5 kPa. Instead, in the upper slab, the elastic module  $E$  is given by the expression presented in the work of Scapozza and Bartelt (2003) as function of the density:

$$E(\rho) = 1.873 \cdot 10^5 \exp^{0.0149\rho} \quad (9)$$

and the tensile strength is taken from Sigrist (2006):

$$\sigma_{yt}^s = 2.4 \cdot 10^5 \left( \frac{\rho}{917} \right)^{2.44} \quad (10)$$

The stresses in the upper slab and in the weak layer can vary over different orders of magnitude. Consequently, we will consider the stress ratio with respect to their threshold, which means that failure will be reached for stress ratio values equal to 1.0 to offer a better understanding of the fracture lengths role and the processes therein.

The first case in analysis considers a density of the upper slab equal to  $280 \text{ kg/m}^3$  as presented in Figure 3. The shear stress ratio  $S_s^w$  in the weak layer reaches the unit value (i.e. fails) just after 11 centimeters of cut length and, at that point, crack propagation starts. On the other side, the upper slab touches the rigid bed at 75 centimeter and the tensile stress ratio  $S_t^s$  changes from a quadratic to a linear growth. This allows the upper slab to remain under the stress threshold, so this case comes up to be full propagation (END) as the crack reaches the end of the specimen.

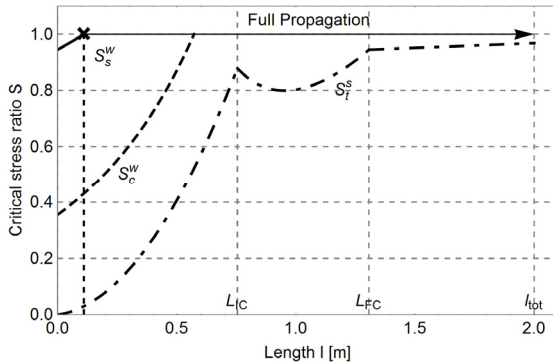


Fig. 3 : Stress evolution for the case of upper slab density  $\rho$  equal to  $280 \text{ kg/m}^3$ , with a full propagation (END) result.

The case of  $230 \text{ kg/m}^3$  density is depicted in Figure 4. Here, the shear stress in the weak layer is responsible for the initial onset of crack propagation, for a 45 centimeters cut. Subsequently, when

the length of the crack is 166 centimeters long, the upper slab fractures under tensile stress. This description corresponds to a slab fracture after propagation case and we denote it with SFa.

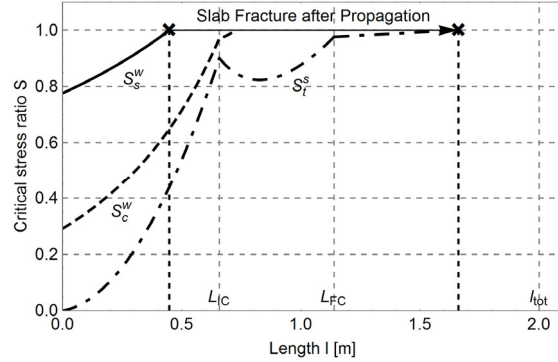


Fig. 4 : Stress evolution for the case of upper slab density  $\rho$  equal to  $230 \text{ kg/m}^3$ , with a slab fracture after propagation (SFa) result.

In the following Figure 5, the upper slab density is set as  $180 \text{ kg/m}^3$ . At first, the upper slab fails at 59 centimeters, causing the reduction of the load in the weak layer. The test is concluded, since no propagation is possible at this point. The slab fracture before propagation is denoted by SFb.

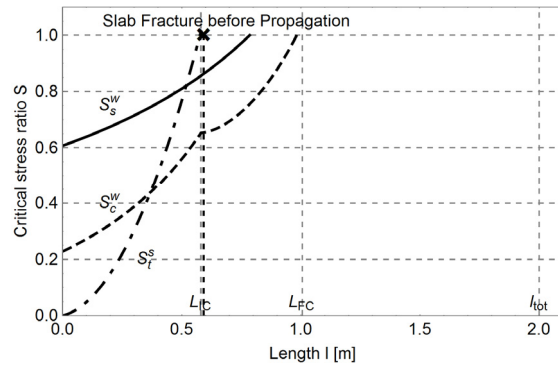


Fig. 5 : Stress evolution for the case of upper slab density  $\rho$  equal to  $180 \text{ kg/m}^3$ , with a slab fracture before propagation (SFb) result.

Finally, the propagation length is computed for the density range  $50$  to  $300 \text{ kg/m}^3$ . Figure 6 shows the resulting plot, where we highlighted the expected test outcome. In relation to soft slabs, up to  $191 \text{ kg/m}^3$ , the slab fractures before any crack propagation is engaged in the weak layer (SFb). Then, as the upper slab becomes stronger than the weak layer, for the range  $191$ - $249 \text{ kg/m}^3$ , slab fracture after propagation (SFa) is predicted. As we previously observed, the propagation length becomes bigger than total length of the specimen (i.e. 2 me-

ters). When the density is higher than  $249 \text{ kg/m}^3$ , the model predicts full propagation (END).

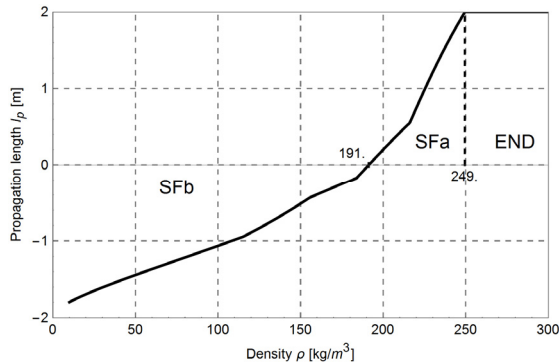


Fig. 6 : Signed propagation length with respect to the density. The slab fracture before propagation (SFb), slab fracture after propagation (SFa) and full propagation (END) results are highlighted in the plot. The total length of the specimen is 2 meters.

This mechanical description of the PST is an advantageous tool for the study of different parameters throughout the test. The analytical solutions can be used to evaluate the sensibility of the model, varying independently each quantity of interest.

#### 4. CONCLUSIONS

This work presented an analytical framework for the mechanical interpretation of the Propagation Saw Test. The Euler-Bernoulli beam theory has been applied to the various stages of the PST, underlining the stress evolution as function of the saw cut length. Moreover, the full propagation (END) and the slab fracture (SFa, SFb) outcomes have been linked with quantitative results, through the computation of the propagation length.

#### ACKNOWLEDGEMENTS

L. Benedetti gratefully acknowledges financial support from the BFW - Austrian Research Centre for Forests, Department of Natural Hazards in Innsbruck as partner in the MuMoLaDe project - Multi-scale Modelling of Landslides and Debris Flows - within the framework of Marie Curie ITN (Initial Training Networks) under the EC 7th Framework Programme.

#### REFERENCES

Gaume, J., van Herwijnen, A., Chambon, G., Birkeland, K. W., and Schweizer, J., 2015: Modeling of crack propagation in the weak snowpack layers using the discrete element method. *The Cryosphere*, 9, 1915-1932.

Gauthier, D. and Jamieson, B., 2008; Evaluation of a prototype field test for fracture and failure propagation propensity in weak snowpack layers. *Cold Regions Science and Technology*, 51, 87-97.

Heierli, J., Gumbsch, P., and Zaiser, M., 2008: Anticrack nucleation as triggering mechanism for snow avalanche. *Science*, 321, 240-243.

Scapozza, C. and Bartelt, P., 2003: Triaxial tests on snow at low strain rate. Part II. Constitutive behavior. *Journal of Glaciology*, 49, 91-101.

Sigrist, C., 2006: *Measurement of Fracture Mechanical Properties of Snow and Application to Dry Snow Slab Avalanche Release*. Ph.D. thesis, ETH Zurich.

Sigrist, C. and Schweizer, J., 2007: Critical energy release rates of weak snowpack layers determined in field experiments. *Geophysical Research Letters*, 34.

Schweizer, J., Reuter, B., van Herwijnen, A., Jamieson, B., and Gauthier, D., 2014: On how the tensile strength of the slab affects crack propagation propensity. *Proceedings of the International Snow Science Workshop*, Banff, Canada, 164-168.

van Herwijnen, A. and Jamieson, B., 2005: High-speed photography of fractures in weak snowpack layers. *Cold Regions Science and Technology*, 43, 71-82.